



Draft Manuscript for Review

Topological shape optimization of multifunctional tissue engineering scaffolds with level set method

Journal:	<i>Structural and Multidisciplinary Optimization</i>
Manuscript ID	SMO-14-0393.R3
Manuscript Type:	Research Paper
Date Submitted by the Author:	n/a
Complete List of Authors:	Wang, Yu; University of Technology, Sydney, School of Electrical, Mechanical and Mechatronic Systems Luo, Zhen; University of Technology, Sydney, School of Electrical, Mechanical and Mechatronic Systems Zhang, Nong; University of Technology, Sydney, School of Electrical, Mechanical and Mechatronic Systems, School of Electrical, Mechanical and Mechatronic Systems Qin, Qinghua; Australian National University, Research School of Engineering
Keywords:	Tissue scaffolds, Microstructure, Topological shape optimization, Level set method

SCHOLARONE™
Manuscripts

view

Submitted to *Structural and Multidisciplinary Optimization*

Original Submission: SMO-14-0393, 09 December 2014;

Revised Submission: SMO-14-0393R1, 07 June 2015;

Revised Submission: SMO-14-0393R2, 15 November 2015;

Revised Submission: SMO-14-0393R3, 24 January 2016;

Topological shape optimization of multifunctional tissue engineering scaffolds with level set method

By

Yu Wang¹, Zhen Luo^{*,1}, Nong Zhang¹, Qinghua Qin²

¹ School of Electrical, Mechanical and Mechatronic Systems
The University of Technology, Sydney, NSW 2007, Australia

² Research School of Engineering
Australian National University, Canberra, ACT 2601, Australia

* Correspondence author:

(Dr Z. Luo, Email: zhen.luo@uts.edu.au; Phone: +61 2 9514 2994; Fax: +61 2 9514 2655)

This paper is submitted for possible publication in *Structural and Multidisciplinary Optimization*. It has not been previously published, is not currently submitted for review to any other journals, and will not be submitted elsewhere during the peer review. It is noted that this manuscript has been submitted in a style of “*Your Paper Your Way*” only for the convenience of peer-review.

ABSTRACT

A tissue engineering scaffold provides a proper environment to support physiological loads, and enhance cell migration and delivery for re-modeling of regenerating tissue. Hence, in the design of scaffolds, it is required to control the scaffold architecture with mechanical and mass transport properties simultaneously. In this paper, a level set-based topology optimization method will be developed to systematically generate three dimensional (3D) microstructures for tissue engineering scaffolds, with the prescribed properties for mechanical stiffness, fluid porosity and permeability. To create the internal architecture for scaffolds with desired properties, the numerical homogenization method will be used to evaluate the effective properties of the microstructure for building the periodic composite media, and a parametric level set method will be introduced to find the optimized shape and topology of the microstructure. Several numerical examples are used to demonstrate the effectiveness of the proposed method in achieving scaffolds with desired multifunctional properties, within the numerically estimated cross-property bounds between the effective bulk modulus and permeability under different porosities.

Keywords: Tissue Scaffolds, Microstructure, Topology optimization, Level set method.

1 INTRODUCTION

In the early 1990s, tissue engineering was mainly developed to overcome the limitations of tissue graft and alloplastic repair [1]. The fundamental essence of tissue engineering is to adapt a porous degradable material called scaffold to transplant bio-factors like stem-cell and gene-therapy approaches, which is used to stimulate tissue repair. Hence, the design of porous biomaterials, such as the scaffold architecture, plays an important role in the tissue regeneration. A basic tissue engineering design hypothesis is that the scaffold should provide a biomimetic mechanical environment for initial function and sufficient porosity for cell migration and cell/gene delivery [2, 3]. To fulfill such multifunctional design requirements, there are several functional characteristics to be considered, such as the porosity, mechanical modulus and permeability/diffusivity. For example, bone tissue engineering scaffolds should be designed to have high diffusivity, permeability or porosity for better cell migration and biologicals transport to meet the multi-criteria requirements [4]. Furthermore, the multifunctional characteristics often vary with the specific tissue. For instance, to maintain the health of bone tissues, taking the trabecular bone as an example, the elastic modulus has a wide range from 10 to 1500 MPa [5]. While, the aggregate modulus for articular cartilages is relatively smaller with a range from 0.5 to 3.0 MPa [6], comparing

1 to that of trabecular bones. Thus, the design challenge of bone tissue engineering scaffolds is actually to explore
2 suitable internal architecture to satisfy their multifunctional properties.
3
4

5 The multifunctional tissue scaffolds are attracting more and more attention in the field of bioengineering, and a
6 number of different design methods [2, 3] have been developed to create scaffolds over the past. More recently,
7 with the rapid development of computational design engineering, topology optimization technique has shown its
8 potential as a powerful design tool for micro-structured scaffolds. Topology optimization [7] is a numerical
9 process to iteratively redistribute a given amount of material to extremize a prescribed objective function under
10 specific constraints, until the best material layout is achieved within a fixed reference domain. Several methods
11 have been developed for topology optimization of structures, such as the homogenization method [8], the SIMP
12 method [9-10], ESO [11] and the level set-based method (LSM) [12-15]. Topology optimization has been
13 applied to design scaffolds to topologically achieve the optimized layout of the microstructure. For instance, Lin
14 and et al. [16] applied the homogenization-based topology optimization method to design 3D internal scaffold
15 architectures, to simultaneously meet the desired elastic properties and porosity for mass transport. Guest and
16 Prevost [17] extended the projection method [18] to topological design of 3D scaffolds, to maximize the bulk
17 modulus and isotropic permeability. Kruijf et al. [19] used topology optimization to generate optimized scaffold
18 structures having maximized bulk modulus and thermal conductivity in two-dimensional (2D) structures based
19 on the Pareto optimality. Challis and et al. [20] developed a level set method to design microstructures with
20 isotropic materials to gain maximized bulk modulus and isotropic conductivity. Challis and et al. [21] also
21 proposed a method for the generation of numerically estimated cross-property bounds for stiffness and fluid
22 permeability porous materials with level sets. Kang [4] applied the homogenization topology optimization to
23 create 3D scaffold architectures, so as to match the desired elastic properties and porosity simultaneously. It is
24 noted that the most of the above topology optimization methods are based on material density distribution.
25
26
27
28
29
30
31
32
33
34
35
36
37
38
39
40
41
42

43 Recently, the LSMs have been emerged as a new family of alternative approached for shape and topology
44 optimization of structures. LSMs were originally developed for tracking, modelling and simulating shape
45 variation of the moving boundary with topological changes by merging and breaking the boundary. LSMs have
46 shown some unique characteristics as a result of the implicit free boundary representation, such as (1) smooth
47 boundary and distinct interface in the process of the optimization, (2) shape fidelity and topological flexibility,
48 and (3) topological changes during shape variations [13,14,22]. However, in conventional LSMs the solution of
49 the Hamilton-Jacobi partial differential equations (H-J PDE) using the finite difference method involves several
50 numerical issues to be carefully handled [23-25], such as the re-initialization of the level set function (LSF), the
51 Courant-Friedrichs-Lewy (CFL) condition, as well as the extension of the normal velocity. Hence, to overcome
52
53
54
55
56
57
58
59
60

the unfavourable numerical features, several alternative LSMs have been developed more recently [22], e.g. the parametric level set method (PLSM) [15], which have been successfully applied to topological shape design of structures [26,27], mechanisms [28] and metamaterials [29]. In PLSM, the key concept is to interpolate the original LSF using a set of compactly supported radial basis function (CS-RBF) [30] to ensure a desirable smoothness and accuracy of the approximation. In this way, the original H-J PDE is changed into a system of equations, and the topological shape optimization is converted to a size optimization, in which the expansion coefficients of the interpolant, which are temporal only, are considered as the design variables. Thus, many more efficient gradient-based optimization algorithms can be directly applied to the optimization problem.

However, the current paper is the first time the original parametric level set method [15] has been extended to a family of more advanced topology optimization problems in a different area of application, namely, topological shape design of three-dimensional (3D) Scaffold microstructures in tissue engineering. In this method, the numerical homogenization method will be used to evaluate the effective property, while the PLSM will be applied to optimize shape and topology of the microstructure by satisfying the prescribed properties, such as mechanical stiffness, fluid porosity and permeability. Several numerical examples are applied to demonstrate the effectiveness of the proposed method in optimizing the 3D tissue engineering scaffolds.

2 HOMOGENIZATION OF ELASTICITY AND PERMEABILITY

In this study, we have the following assumptions: the composite only consists of arrays of periodically arranged microstructures or unit cells; the geometric size of the unit cell is much smaller than the macroscopic material to enable the scale-decomposition in the homogenization; the homogenized effective properties of the composite can be predicted by the mechanical behaviour of the microstructure. Based on the small parameter perturbation of the displacement, the effective properties of the micro-structured scaffold architecture can be computed by using the numerical homogenization method [31].

The effective elasticity tensor C^H relates the macroscopic stress tensor σ to the macroscopic strain tensor ε for the porous biomaterials as follows:

$$\sigma = C^H \varepsilon \quad (1)$$

where C_{ijkl}^H is the effective stiffness tensor, given by

$$C_{ijkl}^H = \frac{1}{|Y|} \int_Y (\varepsilon_{pq}^{0(ij)} - \varepsilon_{pq}^{*(ij)}) C_{pqrs} (\varepsilon_{rs}^{0(kl)} - \varepsilon_{rs}^{*(kl)}) dY \quad (1)$$

and ε^0 is the unit test strain field, $|Y|$ is the volume of the cell, and ε^* is the strains tensor corresponding to the displacement field χ^{kl}

$$\boldsymbol{\varepsilon}_{pq}^{*(kl)} = \frac{1}{2} \left(\frac{\partial \chi_p^{kl}}{\partial y_q} + \frac{\partial \chi_q^{kl}}{\partial y_p} \right) \quad (2)$$

Here χ^{kl} can be obtained by solving the following equation: Find $\chi^{kl} \in U_{period}(Y)$ such that

$$\int_Y C_{ijpq} \frac{\partial \chi_p^{kl}}{\partial y_q} \frac{\partial v_i}{\partial y_j} dY = \int_Y C_{ijpq} \frac{\partial v_i}{\partial y_j} dY \quad \forall v \in U_{period}(Y) \quad (3)$$

where v is the virtual displacement field, $U_{period}(Y)$ is the kinematically admissible displacement space with Y -period. Since the 3D biomaterial with cubic elastic symmetry is considered in this study, this material has an effective stiffness matrix with three independent components of the form

$$\mathbf{C}^H = \begin{bmatrix} C_{11}^H & C_{12}^H & C_{12}^H & 0 & 0 & 0 \\ C_{12}^H & C_{11}^H & C_{12}^H & 0 & 0 & 0 \\ C_{12}^H & C_{12}^H & C_{11}^H & 0 & 0 & 0 \\ 0 & 0 & 0 & C_{44}^H & 0 & 0 \\ 0 & 0 & 0 & 0 & C_{44}^H & 0 \\ 0 & 0 & 0 & 0 & 0 & C_{44}^H \end{bmatrix} \quad (4)$$

The bulk modulus is a commonly used stiffness measure in topology optimization to study the resistance of the material to a volumetric strain. The effective bulk modulus B^H for a material with cubic elastic symmetry is

$$B^H = \frac{1}{3} C_{11}^H + \frac{2}{3} C_{12}^H \quad (5)$$

The permeability for slowly moving incompressible fluids within porous materials can be simulated using the homogenization of Stokes flows through a porous material with Darcy's law on the macroscopic scale

$$\mathbf{U} = -\frac{1}{\mu} \mathbf{K}^H \nabla P \quad (6)$$

where \mathbf{U} is the average fluid velocity, ∇P is the pressure gradient across a porous material, \mathbf{K}^H is the effective fluid permeability tensor and μ is the viscosity of the fluid. In this study, the numerical homogenization method for the fluid follows the method given by Guest and Prévost [17]. By applying the stabilization technique [32] for the Stokes flow and Darcy flow, the effective permeability tensor can be computed as

$$\mathbf{K}^H = [K_{ij}^H] = \frac{1}{|Y|} \mathbf{w}^{(i)\top} \mathbf{K}_{ds} \mathbf{w}^{(i)} \quad (7)$$

where \mathbf{K}^H is the effective fluid permeability, \mathbf{K}_{ds} is Darcy-Stokes viscosity matrix. $\mathbf{w}^{(i)}$ is the velocity vector which can be solved numerically using the stabilized finite element to avoid the Babuska -Brezzi condition [17].

A material with the isotropic flow symmetry has an isotropic effective permeability matrix, which is:

$$\mathbf{K}^H = \begin{bmatrix} K_{11}^H & 0 & 0 \\ 0 & K_{11}^H & 0 \\ 0 & 0 & K_{11}^H \end{bmatrix} \quad (8)$$

The scalar permeability can be computed as follows:

$$k^H = \frac{1}{d} \sum_{i=1}^d K_{ii}^H \quad (9)$$

where d is the dimension and equals to 3 for 3D problems.

3 PARAMETRIC LEVEL SET METHOD

In level set method, the design boundary is implicitly represented as the zero level set of a higher-dimensional level set function (LSF) $\Phi(\mathbf{x})$ [23-25], which is defined over a reference domain $D \subset R^d$ ($d = 2$ or 3). Fig. 1 shows a 2D design boundary represented by a 3D level set surface. The 2D boundary is embedded as follows:

$$\begin{cases} \Phi(\mathbf{x}) > 0 & \forall \mathbf{x} \in \Omega \setminus \partial\Omega & \text{(Solid region)} \\ \Phi(\mathbf{x}) = 0 & \forall \mathbf{x} \in \partial\Omega \cap D & \text{(Design boundary)} \\ \Phi(\mathbf{x}) < 0 & \forall \mathbf{x} \in D \setminus \Omega & \text{(Void region)} \end{cases} \quad (10)$$

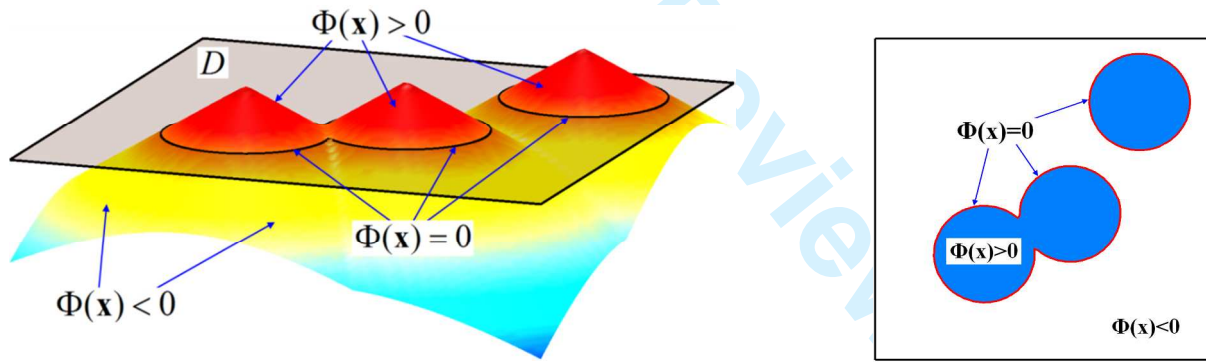


Figure 1 (Left) 3D level set function; (Right) Design domain at the zero level set

To enable the dynamic motion, the pseudo-time t is introduced into the LSF $\Phi(\mathbf{x})$, which leads to the following first-order H-J PDE by differentiating $\Phi(\mathbf{x}, t) = 0$ on both sides with respect to t :

$$\frac{\partial \Phi(\mathbf{x}, t)}{\partial t} + \mathbf{v} \cdot |\nabla \Phi(\mathbf{x}, t)| = 0 \quad (11)$$

where $\mathbf{v} = d\mathbf{x}/dt$ is the velocity field at the design boundary. Only the normal velocity component v_n contributes to the shape evolution of the boundary [13,14], which is expressed as follows:

$$v_n = \mathbf{v} \cdot \mathbf{n} = \mathbf{v} \cdot \left(-\frac{\nabla \Phi}{|\nabla \Phi|} \right) = \frac{d\mathbf{x}}{dt} \cdot \left(-\frac{\nabla \Phi}{\sqrt{\nabla \Phi \cdot \nabla \Phi}} \right) \quad (12)$$

The PLSM [15] has a parameterized level set surface via the interpolation of a given set of CS-RBFs positioned at given knots in the design space, in which the LSF can be expressed as follows:

$$\Phi(\mathbf{x}, t) = \boldsymbol{\varphi}(\mathbf{x})\boldsymbol{\alpha}(t) = \sum_{i=1}^N \varphi_i(\mathbf{x})\alpha_i(t) \quad (13)$$

where the vector of the shape functions (CS-RBF) is defined by

$$\boldsymbol{\varphi}(\mathbf{x}) = [\varphi_1(\mathbf{x}), \varphi_2(\mathbf{x}), \dots, \varphi_N(\mathbf{x})] \in \square^N \quad (14)$$

and the expansion coefficient vector is

$$\boldsymbol{\alpha}(t) = [\alpha_1(t), \alpha_2(t), \dots, \alpha_N(t)]^T \in \square^N \quad (15)$$

where N is the total number of the knots in the design domain.

It can be found that in the parametric level set method, the “parametric” denotes the sampling/interpolation of the original level set function, using the CS-RBF basis functions and the corresponding expansion coefficients at a set of scattered knots or points over the design domain.

The CS-RBFs [30] possess desirable properties in interpolation, including positive definiteness and sparseness of the interpolation matrices under certain conditions, as well as the desired smoothness and continuity of the interpolant. In this work, we will use the following CS-RBF with C2 smoothness (Fig. 2).

$$\varphi_i(r) = \max\{0, (1-r^4)\}(4r+1) \quad (i=1,2,\dots,N) \quad (\text{Wendland-C2}) \quad (16)$$

The above interpolation leads to a separation scheme of the space and time, in which the shape functions are spatial only and the generalized expansion coefficients are time dependent only. The decoupling of the time and space terms of the H-J PDE results in

$$\boldsymbol{\varphi}(\mathbf{x}) \frac{\partial \boldsymbol{\alpha}(t)}{\partial t} - v_n |\nabla \boldsymbol{\varphi}(\mathbf{x})\boldsymbol{\alpha}(t)| = 0 \quad (17)$$

Thus the normal velocity v_n is related to the time derivative of the expansion coefficients $\boldsymbol{\alpha}(t)$ as follows:

$$v_n = \frac{\boldsymbol{\varphi}(\mathbf{x})}{|\nabla \boldsymbol{\varphi}(\mathbf{x})\boldsymbol{\alpha}(t)|} \frac{\partial \boldsymbol{\alpha}(t)}{\partial t} \quad (18)$$

We can find that all the terms involved in v_n are actually evaluated at all the knots in the design domain, and v_n is actually extended to the whole design domain. In this way, the H-J PDE has been parameterized into a system

of equations only with a set of unknowns $\alpha(t)$, which act as the design variables. The propagation of the LSF is just a matter of finding $\alpha(t)$ with an appropriate optimization algorithm. It is noted that there are normally two sets of meshes are involved in level-set based topology optimization methods. The first is to calculate the field quantities (e.g. displacements and strains), and the second is used for propagation of the level set surface.

With the parameterization, the original H-J PDE actually becomes a system of ODEs in which the expansion coefficients are temporal only. However, in the practical numerical implementation, the design variables will be updated sequentially and iteratively using an appropriate optimization algorithm. In this case, from the point of view of iterative optimization, the topological shape optimization problem is essentially changed into a generalized “size” optimization. Here, the “size” refers to the expansion coefficients to be updated under a convergence criterion. In this case, we may say that the “size” optimization problem is similar to SIMP, as the update of the expansion coefficients over the knots is similar to the update of elemental densities in the SIMP.

4 MULTI-OBJECTIVE OPTIMIZATION PROBLEM

Tissue engineering scaffolds are a family of porous biomaterials designed to mainly both bear mechanical loading and enable mass transport. The design of such multifunctional composite materials is actually the multi-objective topology optimization problem.

(1) Material description model using level sets

At an arbitrary point x , the elasticity tensor of the practical material can be given by

$$\mathbf{C}(x) = \mathbf{C}_{\text{base}} H(\Phi(x)) \quad (19)$$

where \mathbf{C}_{base} is the elasticity tensor of the solid material, and H is the Heaviside function, often given as follows:

$$H(\Phi(x)) = \begin{cases} \theta & x < -\Delta \\ \frac{3(1-\theta)}{4} \left(\frac{\Phi(x)}{\Delta} - \frac{\Phi(x)^3}{3\Delta^3} \right) + \frac{1+\theta}{2} & -\Delta \leq x < \Delta \\ 1 & x \geq \Delta \end{cases} \quad (21)$$

where θ is a small positive number (e.g. $1e-4$) to ensure the non-singularity of element stiffness matrix, and Δ is the width for the numerical approximation of the Heaviside function. In the numerical implementation, the Heaviside function is usually smoothed to facilitate the calculation of the first-order derivatives.

For the permeability, the interpolation of the Darcy-Stokes viscosity matrix \mathbf{K}_{ds} is given by

$$\mathbf{K}_{\text{ds}}(x) = \mathbf{K}_{\text{d}} H(\Phi(x)) + \mathbf{K}_{\text{s}} [1 - H(\Phi(x))] \quad (20)$$

where \mathbf{K}_d is Darcy stiffness tensor and \mathbf{K}_s is Stokes stiffness tensor. The above equation denotes that the flow through the solid phase is governed by Darcy's law, while the fluid phase is treated as Stokes flow. Assuming that the design domain with volume $|Y|$, the porosity of material can be calculated as

$$\mathbf{V} = 1 - \frac{1}{|Y|} \int_Y H(\Phi(\mathbf{x})) dY \quad (21)$$

(2) Formulation of the optimization problem using PLSM

In order to achieve the prescribed material properties, the optimization problem is defined as a weighted multi-objective formulation to minimize the error between the prescribed values and the effective values of the bulk modulus and permeability simultaneously, subject to constraints on porosity and symmetric conditions.

$$\left\{ \begin{array}{l} \text{Find} \quad \boldsymbol{\alpha} \\ \text{minimize} \quad J = \omega_B (B^H(\boldsymbol{\alpha}) - B^*)^2 + \omega_k (k^H(\boldsymbol{\alpha}) - k^*)^2 \\ \text{subject to} \quad \mathbf{V}(\boldsymbol{\alpha}) = \mathbf{V}^* \\ \quad \mathbf{g}(\mathbf{C}^H(\boldsymbol{\alpha}), \mathbf{K}^H(\boldsymbol{\alpha})) \leq 0 \\ \quad \mathbf{h}(\boldsymbol{\alpha}) = 0 \end{array} \right. \quad (22)$$

Here $\boldsymbol{\alpha}$ is the vector of design variables, B^* and k^* correspond to the prescribed bulk modulus and permeability of the microstructure, \mathbf{V}^* is the required porosity of the material, and $\mathbf{V}(\boldsymbol{\alpha})$ is the practical porosity of the material. In the numerical implementation, the equality constraint of the porosity can be achieved with a tolerance of 1%. The equality constraint $\mathbf{h}(\boldsymbol{\alpha})=0$ represent the equilibrium equations. The inequalities $\mathbf{g}(B^H(\boldsymbol{\alpha}), k^H(\boldsymbol{\alpha})) \leq 0$ represent the constraints on the effective constitutive tensors, including symmetry constraints. We will consider cubic symmetry for the elastic properties and isotropic symmetry for the flow in the study. ω_B and ω_k are weighting factors used to indicate the relative importance of the two objectives in the design.

In PLSM, the Hamilton-Jacobi PDE driven topological optimization problem has been transformed into a standard parametric optimization problem with a set of generalized "sizes" as the design variables. Actually, the "size" refer to the set of expansion coefficients related to the CS-RBF interpolation. In this case, we do not need to explicitly calculate the normal velocity field \mathbf{v}_n on the level-set boundary and extend the normal velocity field from the boundary to the design domain. However, we still need the expression of the normal velocity field \mathbf{v}_n after the parameterization, because this normal velocity field \mathbf{v}_n will be subsequently used to help derive the design sensitivity together with the shape derivative analysis method and the chain rule.

The derivatives of the C_{ijkl}^H with respect to t is expressed as

$$\frac{dC_{ijkl}^H}{dt} = \frac{1}{|Y|} \int_Y \left(\varepsilon_{pq}^{0(ij)} - \varepsilon_{pq}^* (\chi^{ij}) \right) C_{pqrs} \left(\varepsilon_{rs}^{0(kl)} - \varepsilon_{rs}^* (\chi^{kl}) \right) \delta(\Phi) v_n |\nabla \Phi| dY \quad (23)$$

where $\delta(\Phi)$ is the Dirac function, which is the first-order derivative of the Heaviside function $H(\Phi)$.

Subjecting v_n expressed by Eq. (19) to Eq. (25) leads to

$$\frac{dC_{ijkl}^H}{dt} = \left(\frac{1}{|Y|} \int_Y \left(\varepsilon_{pq}^{0(ij)} - \varepsilon_{pq}^* (\chi^{ij}) \right) C_{pqrs} \left(\varepsilon_{rs}^{0(kl)} - \varepsilon_{rs}^* (\chi^{kl}) \right) \delta(\Phi) \varphi_i(\mathbf{x}) dY \right) \frac{\partial \alpha_i(t)}{\partial t} \quad (26)$$

At the same time, the derivative of C_{ijkl}^H with respect to t can be given as follows by using the chain rule

$$\frac{dC_{ijkl}^H}{dt} = \frac{\partial C_{ijkl}^H}{\partial \alpha_i(t)} \frac{\partial \alpha_i(t)}{\partial t} \quad (24)$$

Comparing the corresponding terms of Eq. (26) and Eq. (27), we can find the sensitivities of C_{ijkl}^H with respect to the design variables α_i by

$$\frac{dC_{ijkl}^H}{d\alpha_i} = \frac{1}{|Y|} \int_Y \left(\varepsilon_{pq}^{0(ij)} - \varepsilon_{pq}^* (\chi^{ij}) \right) C_{pqrs} \left(\varepsilon_{rs}^{0(kl)} - \varepsilon_{rs}^* (\chi^{kl}) \right) \delta(\Phi) \varphi_i(\mathbf{x}) dY \quad (i = 1, 2, \dots, N) \quad (25)$$

Similarly, the sensitivity of K_{kl}^H with respect to the design variables α_i is

$$\frac{dK_{kl}^H}{d\alpha_i} = \frac{1}{|Y|} \int_Y \mathbf{w}^{(i)T} (\delta(\Phi) \mathbf{K}_d - \delta(\Phi) \mathbf{K}_s) \mathbf{w}^{(j)} \varphi_i(\mathbf{x}) dY \quad (i = 1, 2, \dots, N) \quad (26)$$

The sensitivity of the volume constraint (porosity) is given as

$$\frac{dV}{d\alpha_i} = -\frac{1}{|Y|} \int_Y \delta(\Phi) \varphi_i(\mathbf{x}) dY \quad (i = 1, 2, \dots, N) \quad (27)$$

Once the sensitivity information has been obtained, many more efficient optimization algorithms like MMA [33] can be applied to update the design variables (expansion coefficients of the CS-RBF interpolation) iteratively. Then, the interpolant of the level set function will be updated correspondingly, which will lead to the motion of the level set boundary as well as the evolution of the shape and topology of the structure.

(3) Numerical implementation of the topology optimization problem

In the numerical implementation, the ‘‘artificial’’ material model will be used for the solid phase and the periodic boundary condition will be applied to the design domain of the unit cell (microstructure). Geometrical symmetries of the unit cell are considered to achieve cubic elastic symmetric material phase and isotropic flow

1 phase. The standard finite element method (FEM) is employed to discretize the unit cell in order to obtain the
2 displacement field. In this study, the eight-node isoparametric elements will be used to discretize the design
3 domain.
4

5
6 In the conventional SIMP approach, element-wise density variables are usually regarded as the design variables.
7
8 In order to overcome the typical numerical difficulties (e.g. checkerboards), many attempts have been made to
9 formulate the topology optimization problems based on point-wise design variables to evaluate material
10 properties at nodes or meshless points, e.g. [18, 26, 34, 35]. In this study, the material properties are also
11 evaluated at nodes as nodal values. Thus, the LSF is sampled and determined by the interpolation using the CS-
12 RBFs at these nodal positions for the simplicity, as given in Eq. (14). It should be noted that the CS-RBFs knots
13 are not necessarily required to be at the same positions as the element nodes.
14
15
16
17
18
19

20
21 In the level set-based methods, when the boundary crosses an element, it is usually difficult to accurately
22 calculate strain and stiffness of the element. To resolve this problem, there have been several methods available,
23 such as, the widely used “ersatz” model [14]. In this study, an alternative scheme numerically more accurate is
24 applied to evaluate the strain field, based on the computational points ($3 \times 3 \times 3$ Gauss points) of the element. It is
25 a FEM-based alternative scheme, which fully takes advantage of the concept of compactly supported influence
26 domain, e.g. [34, 35]. The material property for each Gaussian point is evaluated by using the interpolation of
27 CS-RBFs and material properties at those nodes located within a compact support domain. The Gaussian points
28 are used as computational points to approximate strain and stiffness of those 3D finite elements cut by the
29 boundary.
30
31
32
33
34
35
36
37

38
39 Then, in the numerical process, the material properties of the Gauss points are determined by the values of the
40 smoothed Heaviside function $H(\Phi)$, which are subsequently applied to assemble the stiffness and Darcy-Stokes
41 viscosity matrices by Eqs. (20) and (22). Namely, the material is assigned to be void/fluid when $H(\Phi)$ takes a
42 small value $\theta = 1e-4$ (the elasticity tensor \mathbf{C} is close to zero, and the Darcy-Stokes viscosity matrix \mathbf{K}_{ds} equals to
43 Stokes stiffness tensor \mathbf{K}_s), and solid when $H(\Phi)$ equals to 1. When $H(\Phi)$ is between $1e-4$ and 1, properties \mathbf{C}
44 and \mathbf{K}_{ds} can be determined according to the interpolation scheme, given in Eqs (20) and (22), respectively.
45
46
47
48
49
50

51
52 The equilibrium equations for the homogenization problem are solved using the FEM to calculate the effective
53 material properties. In the PLSM, the propagation of the LSF is driven by updating the design variables using
54 the Method of Moving Asymptotes (MMA) [33]. To use the gradient-based MMA optimizer, it is necessary to
55 calculate the design sensitivity. The design is iteratively optimized until the change of two successive objective
56
57
58
59
60

function values is less than 0.001, or a maximum of 200 iterations is reached in terms of numerical experience. Compared with the conventional LSMs, in PLSM no re-initialization is required. Moreover, this method is free from the CFL condition, as the topological shape changes is driven by updating the design variables with the MMA, rather than by numerically solving the Hamilton-Jacobi PDE.

5 NUMERICAL EXAMPLES

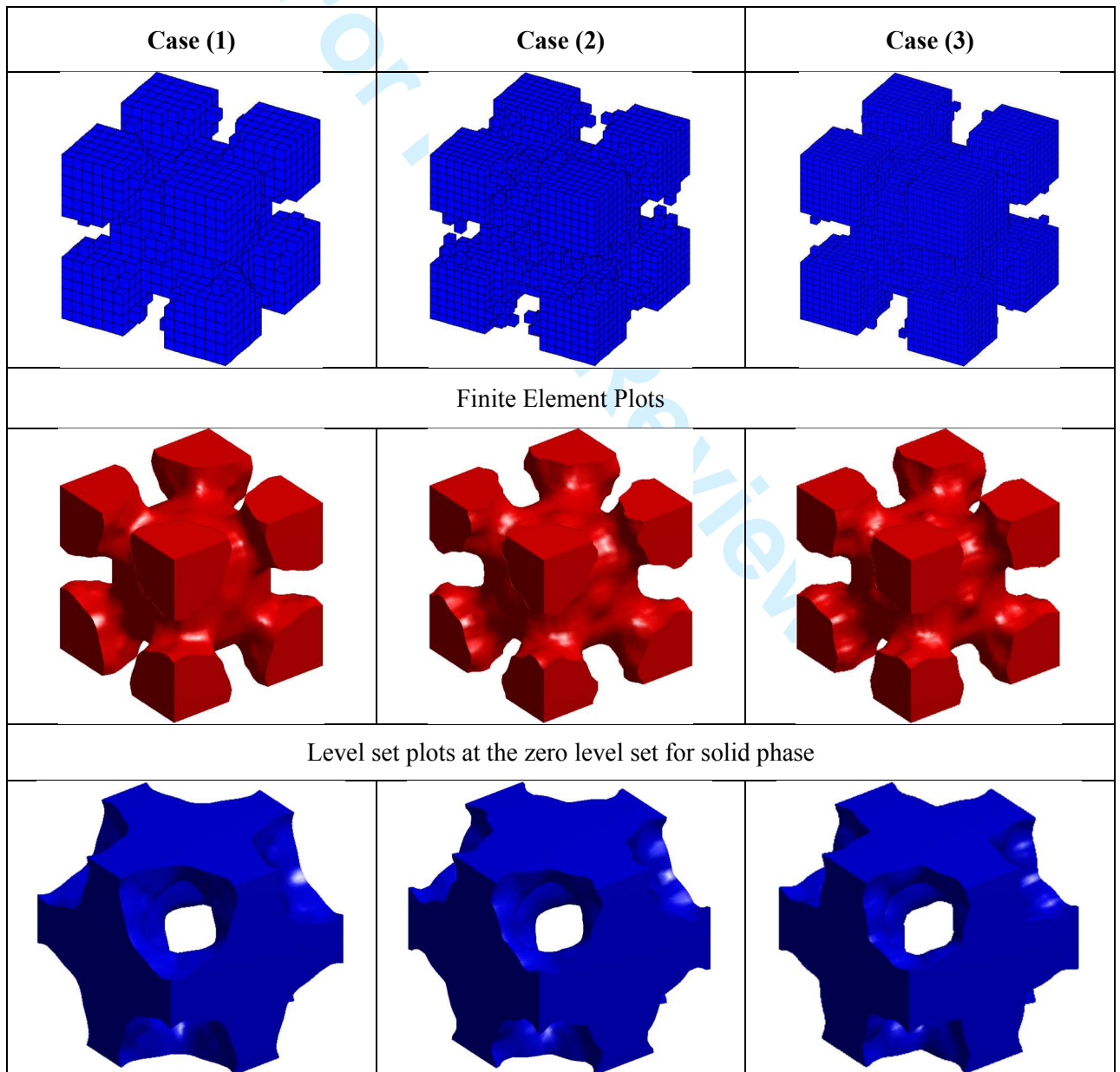
In this section, several numerical examples are used to demonstrate the effectiveness of the proposed approach in designing the scaffold architecture with the prescribed stiffness and mass transport properties. The artificial material is supposed to have Young's modulus $E=1$ and Poisson's ratio $\nu=0.3$. The goal of the design is to achieve target design points with specified effective bulk modulus and permeability within the numerically estimated cross-property upper bounds [21]. The radius of CS-RBF is set to be 2.5 times of the average CS-RBF knots distance (set to be 1) in this study. Different finite element meshes and different porosities will be used to investigate the effectiveness of the proposed optimization method.

(1) Design with different meshes

In this section, the microstructure, with the porosity 50%, the prescribed bulk modulus 0.22 and permeability 0.0005, is optimized under different meshes, e.g. $15 \times 15 \times 15 = 3375$, $20 \times 20 \times 20 = 8000$ and $25 \times 25 \times 25 = 15625$. The optimization parameters and the properties of the microstructure are given in Table 1, and the final results are shown in Figure 2, where the "Finite Element Plots" are actually elemental stiffness plots. More details about this case can be found in Case (f) given in Section (3). The effective element stiffness can be computed based on the properties evaluated at the Gauss points of the element. Elements are plotted when the value of stiffness is larger than a given threshold value (e.g. $0.5 * C_{base}$). It is straightforward to plot the element stiffness. From the finite element plots of the design, it can be found that the optimized topologies are almost the same under the different meshes. Furthermore, with the increase of the number of finite elements, the effective properties of the topologically optimized microstructures change slightly, but more iterations and longer computational time are required for the design to converge.

Based on the final topology at the zero level set, we can find that the boundary of the material phase is smooth and the material interface is distinct. For most numerical approximation methods a finer mesh may be more suitable for a better description of the boundary condition and a better approximation of the field quantities. Hence, a higher meshing resolution may benefit the topological shape description and numerical accuracy, but the computational cost will increase. Here, the mesh size is determined based on our numerical experience.

To save the computational time, the mesh for this numerical case includes $15 \times 15 \times 15 = 3375$ elements. The problem is to design the microstructure under porosity 70% with target effective bulk modulus 0.072 and permeability 0.0028. The convergences of the objective function over iterations are shown in Figure 3. It can be found that the level set method [12-15, 22] has unique features which make the designs including intermediate designs have explicitly trackable smooth boundaries and geometrically distinct interface. Furthermore, we can see that the proposed approach is able to integrate shape optimization and topology optimization as a procedure of topological shape optimization. It is easy to find that the evolution of the topology is completed within the first 40 iterations, and the rest 100 iterations are mainly used to complete the shape variations. Compared with the conventional LSMs (e.g. [14]), the proposed method has been proven to be more efficient and it can find the optimized design normally within 150 iterations.



Level set plots at the zero level set for fluid phase

Figure 2 Optimization results for porosity 50% under different mesh level

Table 1 Optimization parameters and properties of designed microstructures

Case	Meshes	Elements	Computational points	Iterations	Achieved porosity	Achieved bulk modulus	Achieved permeability
(1)	15×15×15	3,375	91,125	136	50.7545%	0.2167	0.000505
(2)	20×20×20	8,000	216,000	199	50.7275%	0.2168	0.000506
(3)	25×25×25	15,625	421,875	195	50%	0.2168	0.000505

(2) Convergence of the design

The convergence history given in Figure 4 shows a case with the same initial design as that of Cases (a) and (h) in next Section. However, the objective of this design is to achieve an effective bulk modulus 0.2 and permeability $2E-5$ under the porosity 50%. After 105 iterations, this optimization process converges at a high effective bulk modulus 0.1981 and a very low permeability $1.8E-5$. Although the nucleation mechanism of new holes in 2D design problem is important, but in 3D designs such mechanism is less important because new holes can be developed by pinching two boundaries (occur without destroying the connectivity of the structure).

Here it is noted that the iteration numbers for a level set-based topology optimization actually depend on the applied formulation: (1) If the standard level set method [13,14] is used, the iteration for the convergence may be over 1000 iterations or even more, due to the time step limitation of the CFL condition; (2) When the discrete level set method, e.g. [36], is used, the iteration for a general convergence criterion will be from 100-200 iterations; (3) For the parametric level set method [15], 200-300 iterations will be normally required for convergence, due to the removal of the time-step limitation of the CFL condition.

Actually, we can flexibly select initial designs for topology optimization problems of structures. It is well known that the same initial structures may lead to different designs if they have been given different objective functions and constraints. Alternatively, different initial structures may generate the same designs for the same optimization problem. In this study, we can find that in some situations the same initial designs can produce the different designs, and sometimes the different designs can lead to different optimized designs, which is further showcase the flexibility on the selection of initial designs for the optimization. Having regard to the design of microstructures, in terms of our numerical experience, we should address that the initial design domain had better involve inhomogeneity of material, so as to facilitate the numerical homogenization method more effectively in estimating the effective properties of the microstructure. It is noted that the locations, shapes and numbers of holes may all have the influence for the approximation of the numerical homogenization method, and as a result effect the optimized designs.

Meanwhile, if an initial design is happened to satisfy the volume constraint, it may enhance the stability of the optimization process and reduce the total numbers of iterations for convergence. It can be found that the different initial microstructures can give different microstructural architecture designs, although the effective properties of the designs may be similar [39]. This phenomenon should be because of multiple local solutions due to non-convexity of the topology optimization problem with the homogenized composite material. Another reason is that for the macro structure consisting of arrays of periodic micro unit cells, each unit cell has periodic boundary condition. The microstructural pattern for repeatedly assembling the macro structure is not unique, depending on how to identify and extract the unit cell from the periodic material, which is found in [16] as well.

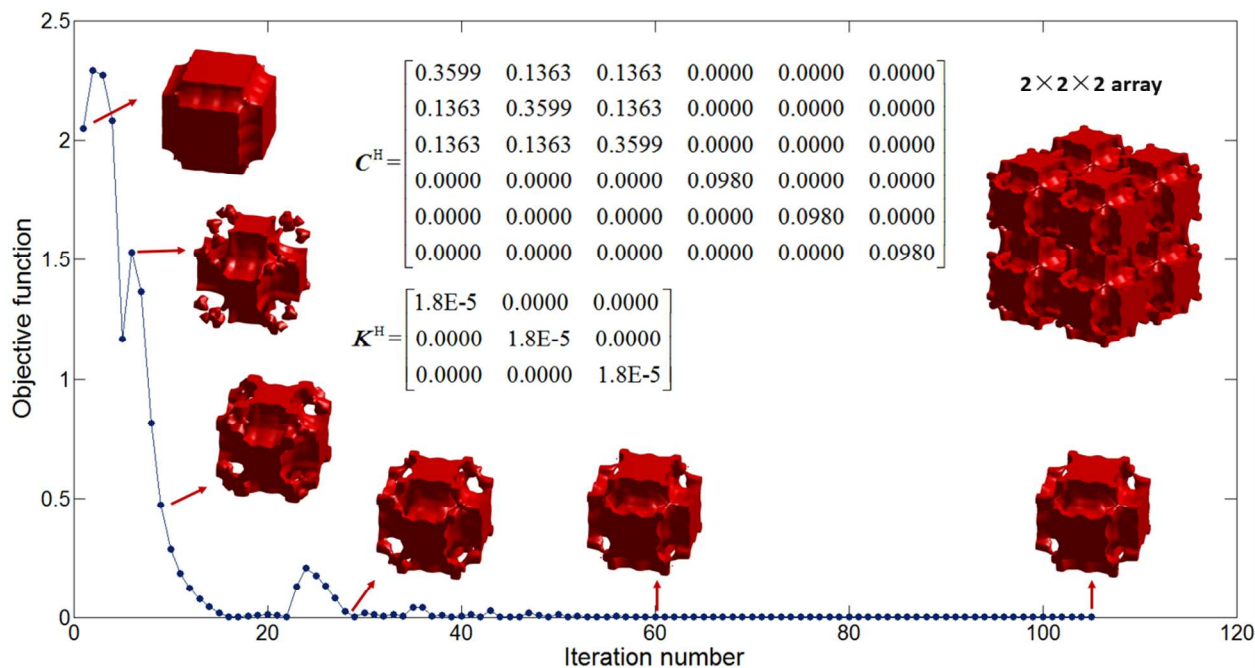


Figure 4. Convergence of the objective function

(3) Designs with different porosities

In this section, we will design microstructures to have a range of effective bulk moduli and permeability values with different porosities. The optimized microstructures with 40%, 50%, and 70% porosities are designed to satisfy the prescribed, numerically estimated cross-property parameters. The optimized material microstructures presented in Table 2-4 are similar to the microstructures given in [17, 37-39]. The parameters for different cases are given in Table 5. The results show how scaffold architecture affects tissue regeneration, since scaffolds can be fabricated to have different stiffness and permeability values for the same porosity.

It should also be noted that for the 3D microstructural design sometimes the final topologies will be similar at the first sight, but their detailed geometric features and fine shapes will be different. This indicates that the final

1 properties of the optimized scaffold are determined not only by the topology but also by local geometrical shape
2 and features of the internal surface, particularly for the design involving the boundary dependent conditions.
3
4

5 As illustrated in Table 2-4, different architectures of scaffold microstructures will give rise to different effective
6 stiffness and permeability even under the same porosities. The porosity plays an important role in determining
7 macroscopic properties of the scaffold as well. The range of stiffness able to be achieved is constrained by the
8 bounds on the effective stiffness derived by Hashin and Shtrikman [40]. Furthermore, from the computational
9 results, it can be seen that the arrangement of holes will effect on the effective permeability. Hollister [2] noted
10 that for a specified scaffold design the effective permeability will decrease with the increase of material, and the
11 effective permeability is only determined by the arrangement of holes. In addition, based on Eq. (8), the value
12 of the effective permeability is dependent on the fluid velocities in the unit cell.
13
14
15
16
17
18
19

20
21 In the topology optimization design, we can also find that higher ratio of porosity for a microstructure indicates
22 the removal of more base material, in order to facilitate a design with more internal pore connections to satisfy
23 the tailored material properties. Under the no-slip condition, the length scales and the total areas of the flow
24 channels have a large effect on the fluid velocities. This explains the phenomenon that Cases (d) and (h), and
25 Cases (f) and (g) have similar topologies but different properties.
26
27
28
29
30
31

32 Since we have achieved a range of effective bulk moduli, the upper Hashin-Shtrikman bound [40] for the bulk
33 modulus will be used to validate the designed scaffold microstructure by using the proposed method. From
34 Figure 5, it can be seen that the bulk modulus of the optimized design are within the upper Hashin-Shtrikman
35 bound. Sigmund [41] also noted that the requirement to maintain mass transport might restrict the optimized
36 microstructure from reaching the upper stiffness bounds. The optimization of stiffness only will lead to a closed
37 unit cell architecture which may approach the upper Hashin-Shtrikman bound [40]. This also explains why the
38 microstructure that is optimized with a fluid conductance constraint cannot reach the upper bounds. Guest [17]
39 investigated the effect of a weighted combination of competing stiffness and flow terms in the objective
40 function, and the numerical results [17] provided a reference for determining the weights in such multi-
41 objective formulation. According to the specific requirements of scaffold design in our study, we found that the
42 stiffness term takes priority in the optimized design.
43
44
45
46
47
48
49
50
51

52
53 The aim of this study is not to achieve maximum effective elastic properties or permeability with a constraint on
54 porosity, but it is to generate new topologically optimized microstructures with desired properties for scaffolds
55 whose properties can match those of natural bone tissue. There are potential applications for topologically
56
57
58
59
60

1 optimized scaffolds with bio material in clinical research. The scaffolds to be used for different positions such
2 as the trabecular bone and cartilage, they should have different properties (e.g. porosity and strength, stiffness,
3 permeability). The optimized microstructure with 40% and 50% porosities and high stiffness can be used for
4 fracture fixation and fusion [16]. For the spinal cage, it requires a scaffold with sufficient load bearing and
5 limited displacement to ensure bone healing [42]. The microstructures like Case (a) and Case (f), which almost
6 reach the upper bound of the effective stiffness, can be considered in this application.
7
8
9
10

11
12 The microstructures with high porosity 70% will be suitable for human trabecular bone such as distal femoral
13 and iliac crest [5]. Scaffold with low stiffness and low permeability are needed for cartilage tissue engineering
14 applications [43]. Such microstructures located within the interior of the cross property bounds and away from
15 the upper limits, such as Case (g) and Case (i), can satisfy the requirements. Since the base material used in this
16 study is artificial, it is difficult to compare the materials properties with those for real-world human tissues.
17
18 Nevertheless, the topologically optimized microstructures with a range of cross properties can still provide a
19 useful reference on how to design the scaffold architectures with controlled material properties.
20
21
22
23
24
25

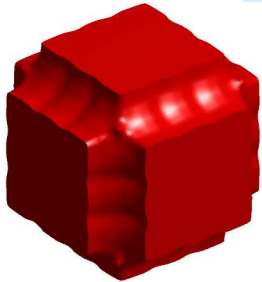
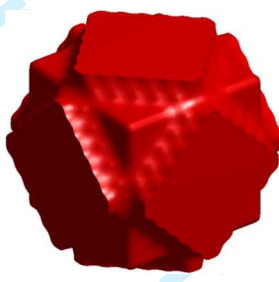
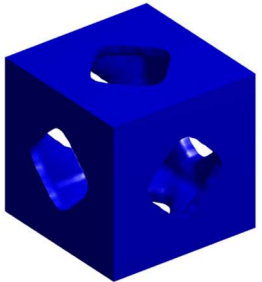
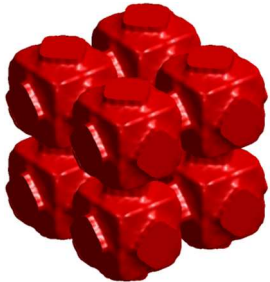
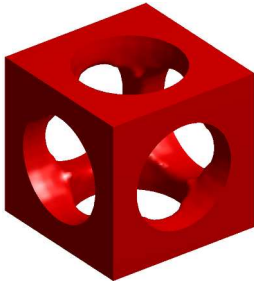
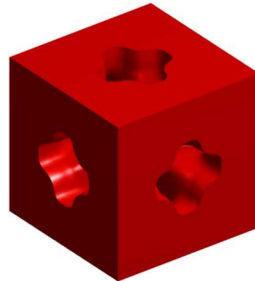
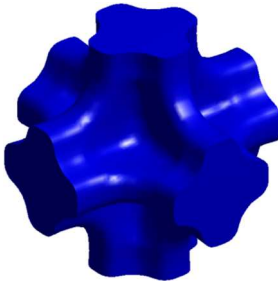
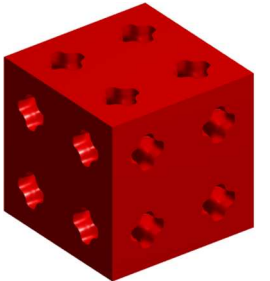
26
27 Furthermore, to validate the numerical results, the properties of the optimized microstructure are compared with
28 the properties of bi-optimal porous materials under cubic elastic and isotropic flow symmetries by Challis and et
29 al [21]. In [21], the bi-optimal porous material design was obtained by setting equal weighting factors in the
30 objective function ($\omega_B = \omega_k = 0.5$). To clarify the comparison, the computational results from [21] (the properties
31 of porous material under different porosities, e.g. 10%, 25%, 50%, 75% and 90%) were plotted as a trend line,
32 shown in Fig. 6. Comparing with the cases in [21], in this work the settings of weights for the objective function
33 and the target properties are different. However, the results in [21] provided the computationally generated
34 cross-property bounds, which can be regarded as references to the achieved effective properties in this work.
35
36
37
38
39
40
41
42

43 In Fig. 6, it can be seen that the properties obtained by the proposed method are reasonably around the bi-
44 optimal cross-property lines. The designed microstructure under the given porosity 50%, namely Case (d),
45 shows a close value of the numerically estimated cross-property and a similar topology as given in [21]. It is
46 noted that the initial structures selected in these two studies are different. Due to the dependency of
47 topologically optimized designs to the initial designs, the topologies of the final structures in these two works
48 are different. Based on the resolutions in this study, it is not surprising to see that the topology optimization
49 design problem under the same porosity may result in fluctuation in material properties. The variance of the
50 effective stiffness can be caused by the different layouts of solid material, while the effective permeability are
51 influenced by the size and shape of the 3D pores and pore connectivity. To meet the multifunctional needs of
52
53
54
55
56
57
58
59
60

scaffold design, the goal of this study is to achieve a range of cross-properties by distributing a given amount of material with different layouts.

From the point of view of scaffold design in tissue engineering [38], tissue growth consideration is an important and challenging problem. In this paper, since the major concern is to develop a systematic design method for the creation of micro-structured mechanical architecture with prescribed material properties to assist scaffold design, we haven't considered the time-dependence of the tissue growth effect in the design of the scaffold. However, in our near future research, we will endeavor to develop a simplified method for design sensitivity analysis involving the time-dependent effect of tissue growth, so as to enable more practical bio engineering applications.

Table 2 Optimized designs of scaffold architecture with the porosity 40%

	Initial guess (Solid phase)	Solid phase	Fluid phase	2×2×2 array
Case (a)				
Parameters of material properties	$C^H = \begin{bmatrix} 0.6311 & 0.2099 & 0.2099 & 0 & 0 & 0 \\ 0.2099 & 0.6311 & 0.2099 & 0 & 0 & 0 \\ 0.2099 & 0.2099 & 0.6311 & 0 & 0 & 0 \\ 0 & 0 & 0 & 0.1698 & 0 & 0 \\ 0 & 0 & 0 & 0 & 0.1698 & 0 \\ 0 & 0 & 0 & 0 & 0 & 0.1698 \end{bmatrix}; \quad K^H = \begin{bmatrix} 0.0035 & 0 & 0 \\ 0 & 0.0035 & 0 \\ 0 & 0 & 0.0035 \end{bmatrix}$			
	Initial guess (Solid phase)	Solid phase	Fluid phase	2×2×2 array
Case (b)				

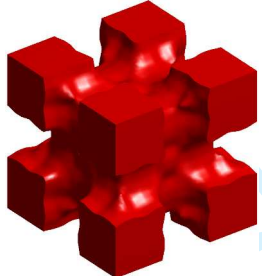
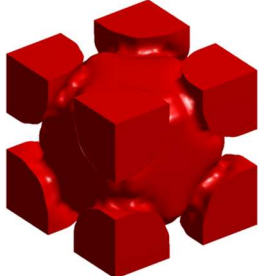
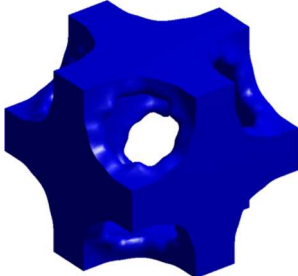
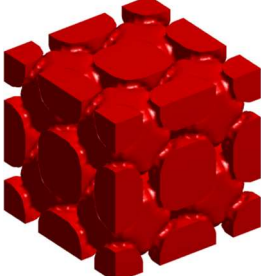
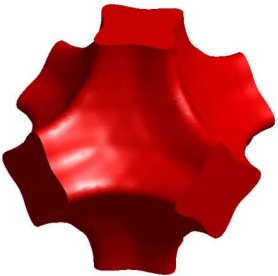
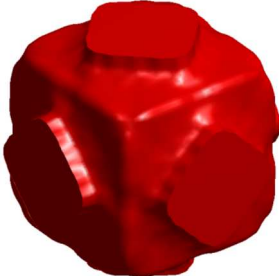
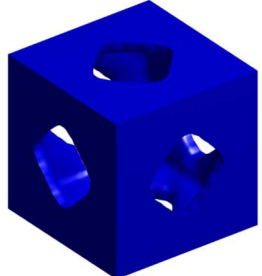
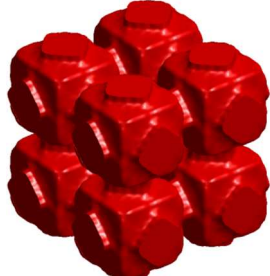
1 2 3 4 5 6 7 8 9 10	Parameters of material properties				$C^H = \begin{bmatrix} 0.5412 & 0.1621 & 0.1621 & 0 & 0 & 0 \\ 0.1621 & 0.5412 & 0.1621 & 0 & 0 & 0 \\ 0.1621 & 0.1621 & 0.5412 & 0 & 0 & 0 \\ 0 & 0 & 0 & 0.1513 & 0 & 0 \\ 0 & 0 & 0 & 0 & 0.1513 & 0 \\ 0 & 0 & 0 & 0 & 0 & 0.1513 \end{bmatrix}; K^H = \begin{bmatrix} 0.3808 \times 10^{-3} & 0 & 0 \\ 0 & 0.3808 \times 10^{-3} & 0 \\ 0 & 0 & 0.3808 \times 10^{-3} \end{bmatrix}$					
11 12 13 14 15 16 17 18 19 20 21	Case (c)	Initial guess (Solid phase)	Solid phase	Fluid phase	2×2×2 array					
22 23 24 25 26 27 28 29 30 31 32										
33 34 35 36 37 38 39 40 41 42 43 44 45 46	Parameters of material properties				$C^H = \begin{bmatrix} 0.4924 & 0.1715 & 0.1715 & 0 & 0 & 0 \\ 0.1715 & 0.4924 & 0.1715 & 0 & 0 & 0 \\ 0.1715 & 0.1715 & 0.4924 & 0 & 0 & 0 \\ 0 & 0 & 0 & 0.1721 & 0 & 0 \\ 0 & 0 & 0 & 0 & 0.1721 & 0 \\ 0 & 0 & 0 & 0 & 0 & 0.1721 \end{bmatrix}; K^H = \begin{bmatrix} 0.0024 & 0 & 0 \\ 0 & 0.0024 & 0 \\ 0 & 0 & 0.0024 \end{bmatrix}$					

Table 3 Optimized designs of scaffold architecture under the porosity 50%

36 37 38 39 40 41 42 43 44 45 46	Case (d)	Initial guess (Solid phase)	Solid phase	Fluid phase	2×2×2 array					
47 48 49 50 51 52 53 54 55										
56 57 58 59 60	Case (e)	Initial guess (Solid phase)	Solid phase	Fluid phase	2×2×2 array					
					$C^H = \begin{bmatrix} 0.3645 & 0.0847 & 0.0847 & 0 & 0 & 0 \\ 0.0847 & 0.3645 & 0.0847 & 0 & 0 & 0 \\ 0.0847 & 0.0847 & 0.3645 & 0 & 0 & 0 \\ 0 & 0 & 0 & 0.0936 & 0 & 0 \\ 0 & 0 & 0 & 0 & 0.0936 & 0 \\ 0 & 0 & 0 & 0 & 0 & 0.0936 \end{bmatrix}; K^H = \begin{bmatrix} 0.007 & 0 & 0 \\ 0 & 0.007 & 0 \\ 0 & 0 & 0.007 \end{bmatrix}$					

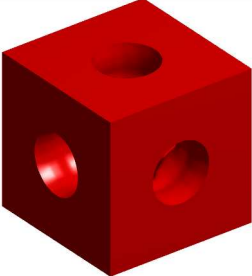
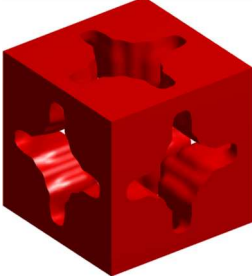
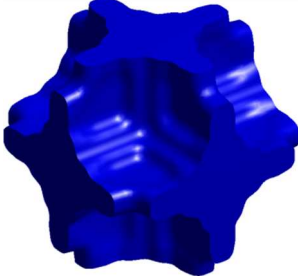
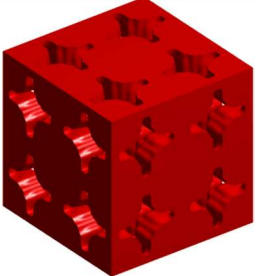
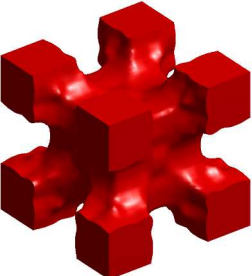
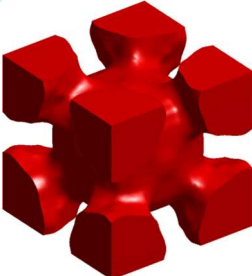
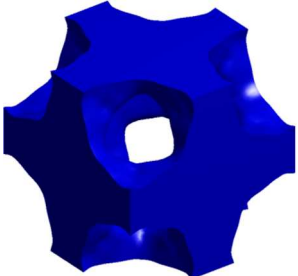
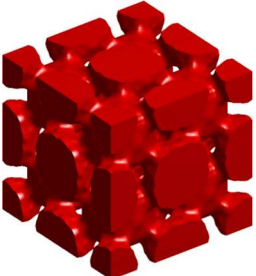
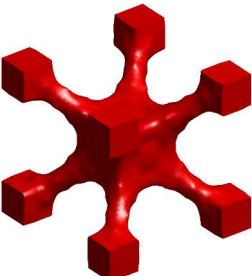
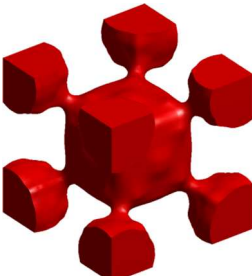
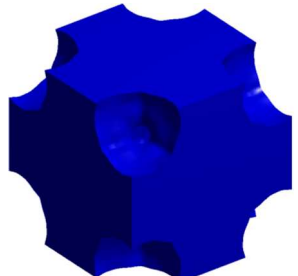
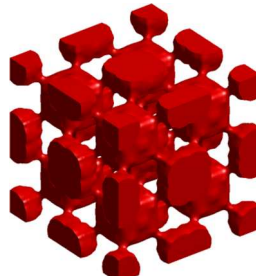
						
Parameters of material properties	$C^H = \begin{bmatrix} 0.1524 & 0.0164 & 0.0164 & 0 & 0 & 0 \\ 0.0164 & 0.1524 & 0.0164 & 0 & 0 & 0 \\ 0.0164 & 0.0164 & 0.1524 & 0 & 0 & 0 \\ 0 & 0 & 0 & 0.0392 & 0 & 0 \\ 0 & 0 & 0 & 0 & 0.0392 & 0 \\ 0 & 0 & 0 & 0 & 0 & 0.0392 \end{bmatrix}; K^H = \begin{bmatrix} 0.008 & 0 & 0 \\ 0 & 0.008 & 0 \\ 0 & 0 & 0.008 \end{bmatrix}$					
Case (f)	Initial guess (Solid phase)	Solid phase	Fluid phase	2×2×2 array		
						
Parameters of material properties	$C^H = \begin{bmatrix} 0.3701 & 0.1387 & 0.1387 & 0 & 0 & 0 \\ 0.1387 & 0.3701 & 0.1387 & 0 & 0 & 0 \\ 0.1387 & 0.1387 & 0.3701 & 0 & 0 & 0 \\ 0 & 0 & 0 & 0.1421 & 0 & 0 \\ 0 & 0 & 0 & 0 & 0.1421 & 0 \\ 0 & 0 & 0 & 0 & 0 & 0.1421 \end{bmatrix}; K^H = \begin{bmatrix} 0.0011 & 0 & 0 \\ 0 & 0.0011 & 0 \\ 0 & 0 & 0.0011 \end{bmatrix}$					

Table 4 Optimized designs of scaffold architecture under the porosity 70%

Case (g)	Initial guess (Solid phase)	Solid phase	Fluid phase	2×2×2 array
				

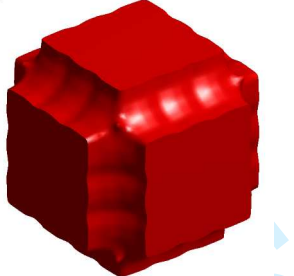
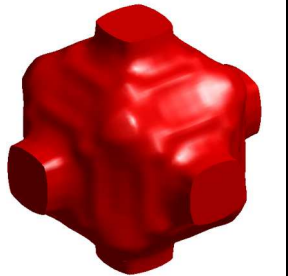
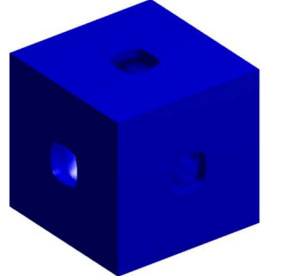
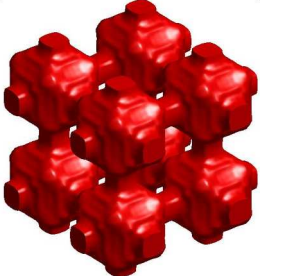
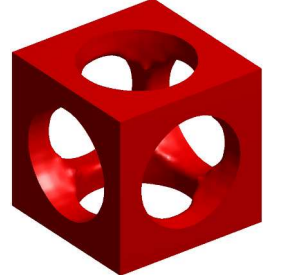
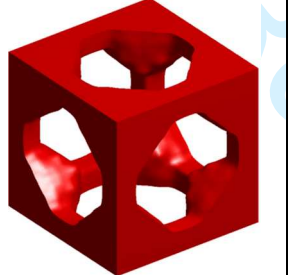
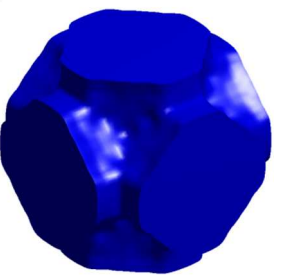
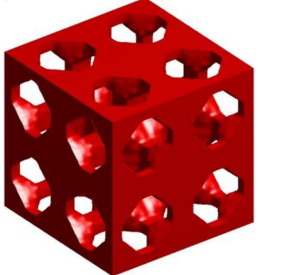
1 2 3 4 5 6 7 8	Parameters of material properties	$C^H = \begin{bmatrix} 0.0979 & 0.0416 & 0.0416 & 0 & 0 & 0 \\ 0.0416 & 0.0979 & 0.0416 & 0 & 0 & 0 \\ 0.0416 & 0.0416 & 0.0979 & 0 & 0 & 0 \\ 0 & 0 & 0 & 0.0534 & 0 & 0 \\ 0 & 0 & 0 & 0 & 0.0534 & 0 \\ 0 & 0 & 0 & 0 & 0 & 0.0534 \end{bmatrix}; K^H = \begin{bmatrix} 4.422 \times 10^{-4} & 0 & 0 \\ 0 & 4.422 \times 10^{-4} & 0 \\ 0 & 0 & 4.422 \times 10^{-4} \end{bmatrix}$					
9 10 11 12 13 14 15 16 17 18 19	Case (h)	Initial guess (Solid phase)	Solid phase	Fluid phase	2x2x2 array		
20							
21 22 23 24 25 26 27 28 29 30	Parameters of material properties	$C^H = \begin{bmatrix} 0.1650 & 0.0208 & 0.0208 & 0 & 0 & 0 \\ 0.0208 & 0.1650 & 0.0208 & 0 & 0 & 0 \\ 0.0208 & 0.0208 & 0.1650 & 0 & 0 & 0 \\ 0 & 0 & 0 & 0.0321 & 0 & 0 \\ 0 & 0 & 0 & 0 & 0.0321 & 0 \\ 0 & 0 & 0 & 0 & 0 & 0.0321 \end{bmatrix}; K^H = \begin{bmatrix} 0.0029 & 0 & 0 \\ 0 & 0.0029 & 0 \\ 0 & 0 & 0.0029 \end{bmatrix}$					
31 32 33 34 35 36 37 38 39 40 41	Case (i)	Initial guess (Solid phase)	Solid phase	Fluid phase	2x2x2 array		
42							
43 44 45 46 47 48 49 50	Parameters of material properties	$C^H = \begin{bmatrix} 0.1960 & 0.0298 & 0.0298 & 0 & 0 & 0 \\ 0.0298 & 0.1960 & 0.0298 & 0 & 0 & 0 \\ 0.0298 & 0.0298 & 0.1960 & 0 & 0 & 0 \\ 0 & 0 & 0 & 0.0379 & 0 & 0 \\ 0 & 0 & 0 & 0 & 0.0379 & 0 \\ 0 & 0 & 0 & 0 & 0 & 0.0379 \end{bmatrix}; K^H = \begin{bmatrix} 2.269 \times 10^{-4} & 0 & 0 \\ 0 & 2.269 \times 10^{-4} & 0 \\ 0 & 0 & 2.269 \times 10^{-4} \end{bmatrix}$					

Table 5 Initial parameters and corresponding optimized results

Case	(ω_B, ω_k)	B^*	k^*	B^H	k^H
(a)	(1.00, 0.2)	0.2	0.005	0.3369	0.0035
(b)	(1.00, 0.1)	0.28	0.001	0.2849	0.0003808

(c)	(1.00, 0.2)	0.26	0.005	0.2786	0.0024
(d)	(1.00, 0.5)	0.18	0.005	0.18	0.007
(e)	(1.00, 0.5)	0.1	0.01	0.0693	0.008
(f)	(1.00, 0.02)	0.22	0.002	0.2167	0.0011
(g)	(1.00, 0.02)	0.06	0.001	0.0643	0.0004422
(h)	(1.00, 0.02)	0.07	0.005	0.0726	0.0029
(i)	(1.00, 0.02)	0.085	0.0005	0.0879	0.0002669

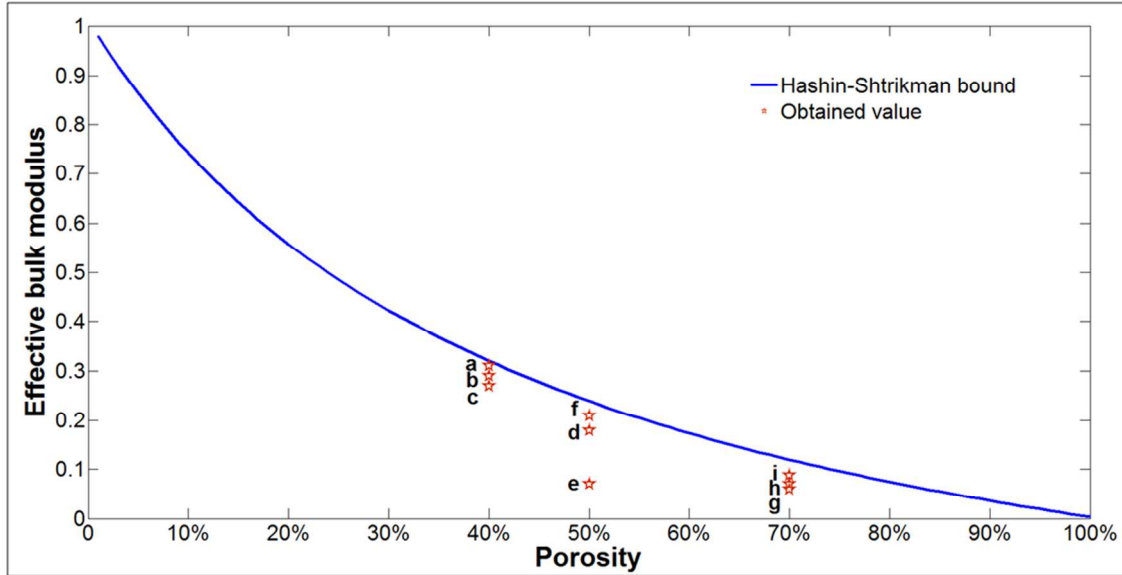


Figure 5 Comparison of the achieved properties with the upper Hashin-Shtrikman bound [37]

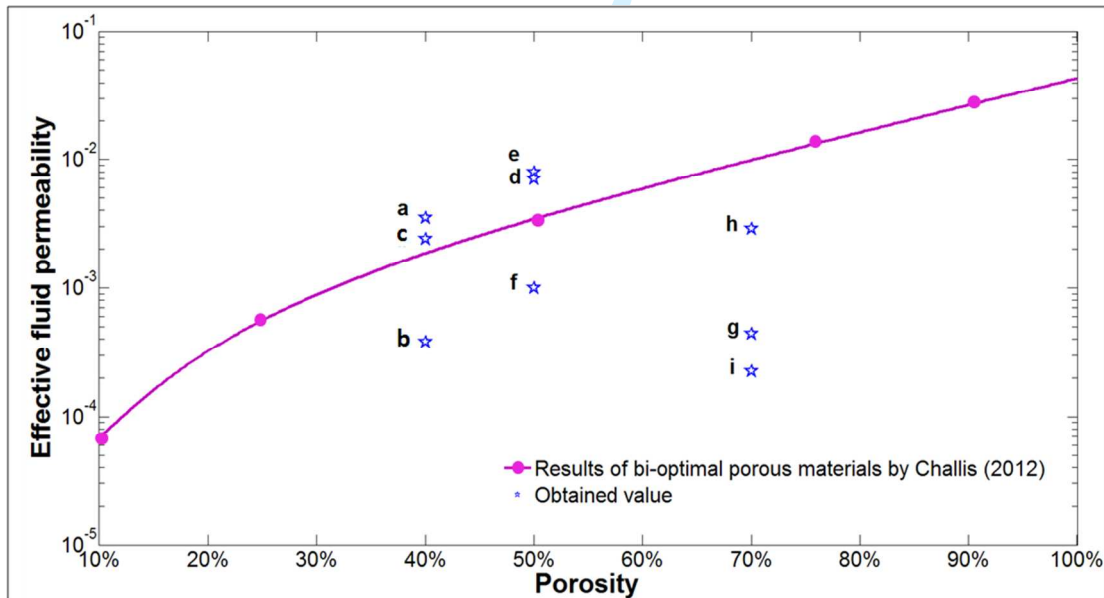


Figure 6 Comparison of the achieved properties with the results of Challis (2012) [21]

6 CONCLUSIONS

This paper has developed a systematic computational design method to generate micro-structured architectures using a multiphase level set method for 3D scaffolds in tissue engineering to achieve multifunctionality, e.g. mechanical stiffness, fluid porosity and permeability. The numerical homogenization method is integrated into the PLSM to optimize shape and topology of the microstructure. Several numerical examples have been applied to demonstrate the effectiveness of the proposed method. Moreover, the final microstructure is geometrically characterized with smooth boundaries and distinct material interfaces, which may greatly facilitate fabrication of the topologically optimized scaffolds which normally have complex geometries and shapes. From the results, we can see that the proposed method can be used to generate a range of different scaffold architectures with various stiffness, porosity and permeability, to satisfy the multifunctionality of tissue engineering scaffolds. It is noted that the proposed method can be extended to more advanced design problems for scaffolds.

ACKNOWLEDGEMENTS

This research is supported in part by the Australian Research Council (ARC)-Discovery Project (DP160102491, DP150102751), the National Natural Science Foundation of China (51575204), and the Science and Technology Support Program of Hubei Province of China (2015BHE026), as well as by the Open Research Foundation of State Key Lab. of Digital Manufacturing Equipment & Technology (DMETKF2015010), Huazhong University of Science & Technology, Wuhan, China.

REFERENCES

- [1] Lanza R, Langer R, and Vacanti JP. Principles of tissue engineering. Academic press; 2011.
- [2] Hollister SJ. Porous scaffold design for tissue engineering. *Nature Materials* 2005; 4:518-524.
- [3] Hollister SJ, Maddox RD, and Taboas JM. Optimal design and fabrication of scaffolds to mimic tissue properties and satisfy biological constraints. *Biomaterials* 2002; 23:4095-4103.
- [4] Kang H, Lin CY, and Hollister SJ. Topology optimization of three dimensional tissue engineering scaffold architectures for prescribed bulk modulus and diffusivity. *Structural and Multidisciplinary Optimization* 2010; 42:633-644.
- [5] Goulet RW, et al. The relationship between the structural and orthogonal compressive properties of trabecular bone. *Journal of Biomechanics* 1994; 27:375-389.
- [6] Boschetti F, et al. Biomechanical properties of human articular cartilage under compressive loads. *Biorheology* 2004; 41:159-166.
- [7] Bendsoe MP, and Sigmund O. Topology optimization: theory, methods, and applications. Springer, Berlin Heidelberg, 2003.
- [8] Bendsoe MP and Kikuchi N. Generating optimal topologies in structural design using a homogenization method. *Computer Methods in Applied Mechanics and Engineering* 1988; 71:197-224.

- 1 [9] Zhou M, Rozvany GIN. The COC algorithm, Part II: topological, geometry and generalized shape
2 optimization, *Computer Methods in Applied Mechanics and Engineering* 1991; 89:197-224.
- 3 [10] Bendsøe MP and Sigmund O. Material interpolation schemes in topology optimization. *Archive of*
4 *Applied Mechanics* 1999; 69:635-654.
- 5 [11] Xie YM and Steven GP. A simple evolutionary procedure for structural optimization. *Computers &*
6 *Structures* 1993; 49: 885-896.
- 7 [12] Sethian JA and Wiegmann A. Structural boundary design via level set and immersed interface methods.
8 *Journal of Computational Physics* 2000; 163:489-528.
- 9 [13] Wang MY, Wang X, and Guo D. A level set method for structural topology optimization. *Computer*
10 *Methods in Applied Mechanics and Engineering* 2003; 192: 227-246.
- 11 [14] Allaire G, Jouve F, and Toader A-M. Structural optimization using sensitivity analysis and a level-set
12 method. *Journal of Computational Physics* 2004; 194:363-393.
- 13 [15] Luo Z, Wang MY, Wang S, and Wei P. A level set-based parameterization method for structural shape
14 and topology optimization. *International Journal for Numerical Methods in Engineering* 2008; 76:1-26.
- 15 [16] Lin CY, Kikuchi N, and Hollister SJ. A novel method for biomaterial scaffold internal architecture
16 design to match bone elastic properties with desired porosity. *Journal of Biomechanics* 2004; 37: 623-
17 636.
- 18 [17] Guest JK and Prévost JH. Optimizing multifunctional materials: Design of microstructures for
19 maximized stiffness and fluid permeability. *International Journal of Solids and Structures* 2006; 43:
20 7028-7047.
- 21 [18] Guest JK, Prévost JH, and Belytschko T. Achieving minimum length scale in topology optimization
22 using nodal design variables and projection functions. *International Journal for Numerical Methods in*
23 *Engineering* 2004; 61: 238-254.
- 24 [19] de Kruijf N, Zhou S, Li Q, and Mai YW. Topological design of structures and composite materials with
25 multiobjectives. *International Journal of Solids and Structures* 2007; 44: 7092-7109.
- 26 [20] Challis VJ, Roberts AP, and Wilkins AH. Design of three dimensional isotropic microstructures for
27 maximized stiffness and conductivity. *International Journal of Solids and Structures* 2008; 45:4130-
28 4146.
- 29 [21] Challis VJ, Guest JK, Grotowski JF, and Roberts AP. Computationally generated cross-property bounds
30 for stiffness and fluid permeability using topology optimization. *International Journal of Solids and*
31 *Structures* 2012; 49:3397-3408.
- 32 [22] van Dijk NP, Maute K, Langelaar M, van Keulen F. Level-set methods for structural topology
33 optimization: a review, *Structural and Multidisciplinary Optimization* 2013; 48: 437-472.
- 34 [23] Osher S, and Sethian JA. Fronts propagating with curvature-dependent speed: Algorithms based on
35 Hamilton-Jacobi formulations. *Journal of Computational Physics* 1988; 79: 12-49.
- 36 [24] Sethian JA. Level set methods and fast marching methods: Evolving interfaces in computational
37 geometry, fluid mechanics, computer vision, and materials science. Cambridge University; 1999.
- 38 [25] Osher S, Fedkiw R.P., Level set methods and dynamic implicit surface, Springer, New York, 2002.
- 39 [26] Luo Z, Zhang N, Gao W, Ma H. Structural shape and topology optimization using a meshless Galerkin
40 level set method. *International Journal for Numerical Methods in Engineering* 2012; 90 (3), 369-389.
- 41 [27] Wang YQ, Luo Z, Kang Z, Zhang N. A multi-material level set-based topology and shape optimization
42 method. *Computer Methods in Applied Mechanics and Engineering* 2015; 283: 1570-1586.
- 43
44
45
46
47
48
49
50
51
52
53
54
55
56
57
58
59
60

- 1 [28] Luo Z, Zhang N, Ji J, Wu T. A meshfree level-set method for topological shape optimization of
2 compliant multiphysics actuators. *Computer Methods in Applied Mechanics and Engineering* 2012; 223-
3 224: 133-152.
- 4 [29] Wang YQ, Luo Z, Zhang N, and Kang Z. Topological shape optimization of microstructural
5 metamaterials using a level set method. *Computational Materials Science* 2014; 87:178-186.
- 6 [30] Wendland H. Computational aspects of radial basis function approximation. *Studies in Computational*
7 *Mathematics* 2006; 12:231-256.
- 8 [31] Guedes J, Kikuchi N, Preprocessing and postprocessing for materials based on the homogenization
9 method with adaptive finite element methods. *Computer Methods in Applied Mechanics and*
10 *Engineering* 1990; 83: 143-198.
- 11 [32] Hughes TJR, Franca LP, and Balestra M. A new finite element formulation for computational fluid
12 dynamics: V. Circumventing the babuška-brezzi condition. *Computer Methods in Applied Mechanics*
13 *and Engineering* 1986; 59: 85-99.
- 14 [33] Svanberg K. The method of moving asymptotes-a new method for structural optimization. *International*
15 *Journal for Numerical Methods in Engineering* 1987; 24: 359-373.
- 16 [34] Kang Z and Wang Y. Structural topology optimization based on non-local Shepard interpolation of
17 density field. *Computer Methods in Applied Mechanics and Engineering* 2011; 200: 3515-3525.
- 18 [35] Luo Z, Zhang N, Wang Y, and Gao W. Topology optimization of structures using meshless density
19 variable approximants, *International Journal for Numerical Methods in Engineering* 2013; 93: 443-464.
- 20 [36] Challis VJ, A discrete level-set topology optimization code written in Matlab. *Structural and*
21 *Multidisciplinary Optimization* 2010;41: 453-464.
- 22 [37] Chen YH, Zhou SW, and Li Q. Computational design for multifunctional microstructural composites.
23 *International Journal of Modern Physics B*, 2009; 23: 1345-1351
- 24 [38] Chen YH, Zhou SW, and Li Q. Microstructure design of biodegradable scaffold and its effect on tissue
25 regeneration. *Biomaterials* 2011; 32: 5003-5014.
- 26 [39] Guedes JM, Rodrigues HC, and Bendsøe MP. A material optimization model to approximate energy
27 bounds for cellular materials under multiload conditions. *Structural and Multidisciplinary Optimization*
28 2003; 25:446-452.
- 29 [40] Hashin Z and Shtrikman S. A variational approach to the theory of the elastic behaviour of multiphase
30 materials. *Journal of the Mechanics and Physics of Solids* 1963; 11:127-140.
- 31 [41] Sigmund O. On the optimality of bone microstructure. Neverland: Springer; 2002.
- 32 [42] Lin CY and Hollister SJ, An integrated global layout and local microstructure topology optimization
33 approach for spinal cage design and fabrication. *Proceedings of the 29th Annual Meeting of*
34 *Biomaterials*, Reno, NV, USA
- 35 [43] Kelly DJ and Prendergast PJ, Prediction of the optimal mechanical properties for a scaffold used in
36 osteochondral defect repair. *Tissue engineering* 2006; 12: 2509-2519.
- 37
38
39
40
41
42
43
44
45
46
47
48
49
50
51
52
53
54
55
56
57
58
59
60